Special Issue: V3-LAVA PROJECT

The HOTSAT volcano monitoring system based on combined use of SEVIRI and MODIS multispectral data

Gaetana Ganci[1,*], Annamaria Vicari[1], Luigi Fortuna[2], Ciro Del Negro[1]

[1] *Istituto Nazionale di Geofisica e Vulcanologia, Sezione di Catania, Osservatorio Etneo, Catania, Italy*

[2] *Università di Catania, Dipartimento di Ingegneria Elettrica, Elettronica e Informatica (DIEEI), Catania, Italy*

Article history
Received February 7, 2011; accepted June 15, 2011.
Subject classification:
Etna volcano, Infrared remote sensing, MODIS, SEVIRI.

ABSTRACT

Spaceborne remote sensing of high-temperature volcanic features offers an excellent opportunity to monitor the onset and development of new eruptive activity. To provide a basis for real-time response during eruptive events, we designed and developed the volcano monitoring system that we call HOTSAT. This multiplatform system can elaborate both Moderate Resolution Imaging Spectroradiometer (MODIS) and Spinning Enhanced Visible and Infrared Imager (SEVIRI) data, and it is here applied to the monitoring of the Etna volcano. The main advantage of this approach is that the different features of both of these sensors can be used. It can be refreshed every 15 min due to the high frequency of the SEVIRI acquisition, and it can detect smaller and/or less intense thermal anomalies through the MODIS data. The system consists of data preprocessing, detection of volcano hotspots, and radiative power estimation. To locate thermal anomalies, a new contextual algorithm is introduced that takes advantage of both the spectral and spatial comparison methods. The derivation of the radiative power is carried out at all 'hot' pixels using the middle infrared radiance technique. The whole processing chain was tested during the 2008 Etna eruption. The results show the robustness of the system after it detected the lava fountain that occurred on May 10 through the SEVIRI data, and the very beginning of the eruption on May 13 through the MODIS data analysis.

1. Introduction

The frequent and synoptic view afforded by satellite-based sensors provides an excellent means to monitor the thermal activity of a volcano by offering adaptability and repeatability, while minimizing exposure to potential volcanic hazards [Francis and Rothery 2000, Harris et al. 2007]. In the past, data provided by the Landsat high spatial resolution and low temporal resolution (16 days) have been used for the thermal analysis of active lava flows [Oppenheimer 1991], lava domes [Francis and McAllister 1986, Kaneko et al. 2002], lava lakes [Harris et al. 1999] and fumarole fields [Harris and Stevenson 1997]. Thermal measurements have been shown to be particularly suited for the detection of the onset of volcanic eruptions [Francis and Rotery 1987, Harris et al. 1995], for the mapping of total thermal flux from active lava flows with high refreshing rates [Flynn et al. 1994, Harris et al. 1998], and to provide preliminary estimates of effusion rates to drive lava flow simulators [Hérault et al. 2009, Vicari et al. 2009].

Even though high spatial resolution images can provide useful information for detailed characterization of the thermal properties of a volcano, images with lower spatial but higher temporal resolution can be acquired by meteorological satellites. Such images have proven to provide a suitable instrument for continuous monitoring of volcanic activity, although the relevant volcanic characteristics are much smaller than the nominal pixel size [Harris et al. 1997, Harris et al. 2000, Wright et al. 2001, Wright et al. 2004]. Indeed, sensors aboard meteorological satellites, such as the Moderate Resolution Imaging Spectroradiometer (MODIS) and the Spinning Enhanced Visible and Infrared Imager (SEVIRI), can detect emitted radiance in the shortwave infrared (SWIR) part of the electromagnetic spectrum, a region in which active lava flows, vents and domes emit copious amounts of energy.

MODIS offers up to 10 wavebands that are suitable for hotspot detection, and being aboard the Terra (EOS AM) and Aqua (EOS PM) polar satellites, it can provide data at least four times a day for any subaerial volcano, with a spatial resolution of about 1 km. In particular, band 21, which is also known as the 'fire channel', was designed to have a much higher saturation temperature of about 500 K [Kaufman et al. 1998]. For these reasons, MODIS data have been used as the basis for automated systems for the detection and monitoring of volcanic eruptions over the entire globe [Wright et al. 2002].

New opportunities for near real-time volcano monitoring came with the launch of SEVIRI, in August 2002, onboard the MSG1 and MSG2 geosynchronous platforms.

Indeed, in spite of the low spatial resolution (3 km at nadir), the frequency of observations provided by the MSG SEVIRI for images at 15-minute intervals was recently applied both for fire detection [Laneve and Cadau 2009] and for the monitoring of effusive volcanoes in Europe and Africa [Hirn et al. 2008].

Since the MODIS and SEVIRI data show significantly different characteristics in spatial, spectral and temporal resolution, the aim of this study was to integrate the information coming from both of these sensors to obtain a better understanding of the volcanic phenomenon. To this end, a multi-platform tool for satellite image analysis and volcanic process characterization is presented here. Computing routines were designed to enable the joint exploitation of MODIS and SEVIRI radiometers in operational monitoring, as a response to the need for fast and robust hotspot detection and radiant flux estimation at active volcanoes. This monitoring system was applied during the 2008 Mount Etna eruption, when it provided identifying pixels that covered the lava flow and processed these pixels to compute their radiative power.

2. The HOTSAT multiplatform system

Analyzing satellite imagery collected from multiple sensors and/or multiple platforms is a common technique that has been used to increase the sampling frequency of observations, to validate the performance of detection algorithms, and to cross-calibrate measurements such as radiative power [Wooster et al. 2003, Hirn et al. 2005, Freeborn et al. 2009]. The multi-platform approach takes advantages of integrating information coming from sensors with different spatial, spectral and temporal resolutions. HOTSAT is essentially composed of three packages: pre-processing, product generation, and post-processing (see Figure 1).

The pre-processing module is necessary for initial geolocation and calibration of the satellite images.

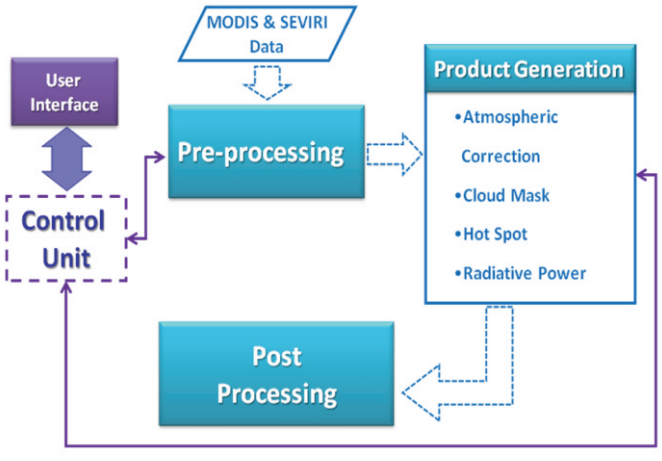

Figure 1. Scheme of the HOTSAT volcano monitoring system.

The product generation block computes higher-level products from the satellite band data. It includes hotspot detection and radiative power estimation.

The post-processing module projects raw geometry data to a cartographic reference system, and exports the derived image files as standard DTP formats (e.g. bmp, jpeg, gif).

This entire package is managed by a control unit, and the user can configure these settings. In the following sections, the main aspects of the HOTSAT system are illustrated.

2.1 The hotspot detection algorithm

The automatic detection of hotspots is not a trivial question, as an appropriate threshold radiance value must be chosen to distinguish the pixels that contain hotspots from those that do not. Traditional algorithms rely on simple threshold tests and questions can arise concerning the correct choice of the thresholds, based on latitude, season and time of day.

Threshold algorithms such as the normalized thermal index [NTI; Wright et al. 2002], which has proven successful for MODIS, did not show comparable results when applied to SEVIRI. Evidence of this can be seen from Figure 2, where the NTI values are given for the South East Crater (SEC) in May 2008. Here we have also plotted the thresholds that can be used to classify a pixel as hot (i.e. –0.8 for night-time, and -0.6 for day-time) [from Wright et al. 2002]. The 2008 Etna eruption started on May 13 and was preceded by a lava fountain on May 10: from this index we can distinguish the lava fountain and the first strong phase of activity that reached a maximum on May 15 and then rapidly decreased to May 19. Although the eruption continued with an active lava flow, according to the NTI, after May 19 no thermal anomaly was detected (Figure 2).

To overcome such limitations due to a fixed threshold, we introduce a new contextual algorithm based on a dynamic threshold and apply it to both the MODIS and SEVIRI data. The HOTSAT hotspot detection algorithm takes as its starting point the contextual approach of Harris et al. [1995] [i.e. the VAST code of Higgins and Harris 1997], and uses the difference between brightness temperature in the middle infrared radiance (MIR) and the thermal infrared radiance (TIR), as ΔTdiff, while setting a threshold ΔT obtained from within the image to define whether a pixel is 'potentially' hot. This threshold is computed by taking into account the spatial standard deviation of the ΔTdiff for each pixel.

The algorithm thus first defines a 'nonvolcanic' portion of the image and uses the maximum ΔT from that portion to set the threshold. Pixels belonging to the volcanic area are then scanned and all of the pixels that show a ΔTdiff greater than the threshold are classified as 'potentially' hot. The

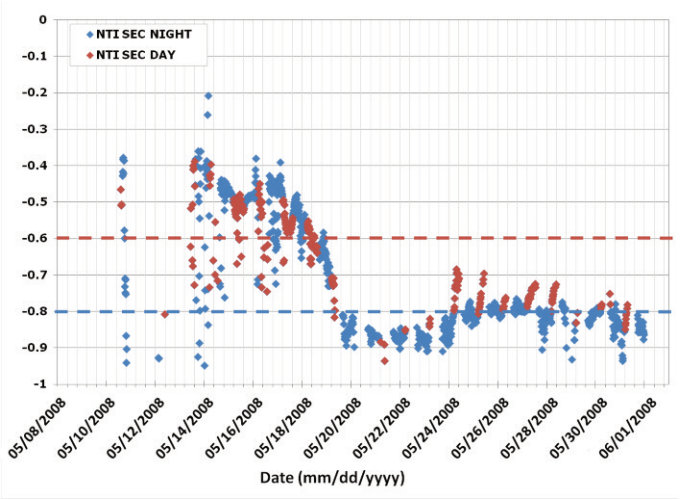

Figure 2. Normalized thermal index sequence computed for the SEVIRI data at the SEC. Red dots, day images; blue dots, night images.

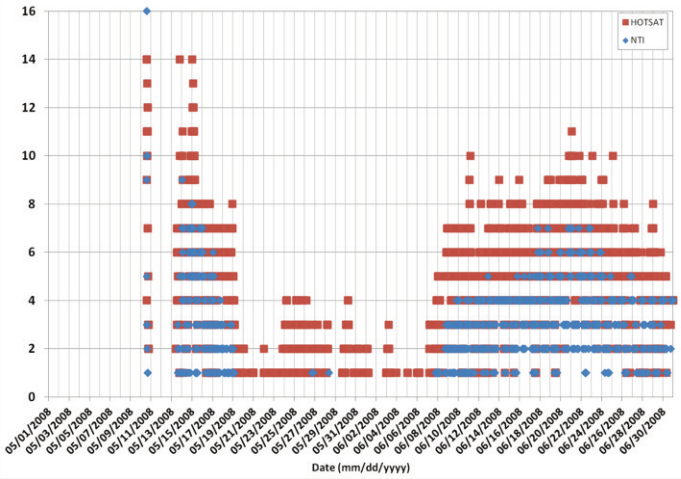

Figure 3. Hotspot numbers detected by the normalized thermal index algorithm (blue) and the HOTSAT hotspot detection algorithm (red), during May and June, 2008, for the SEVIRI data.

algorithm then analyzes all of these 'potentially' hot pixels and their neighbors, to further assess these pixels as true or false hotspot detection, based on a threshold test derived from the statistical behavior of the 3.9 μm brightness temperatures.

Indeed the 'potentially' hot pixels and their neighbors are classified as hot if at least one of the following two conditions is met:

$$T_{3.9\mu m} - \min(T_{3.9\mu m}) > \mathrm{MaxVar}(T_{3.9\mu m}) \quad (1)$$

$$T_{3.9\mu m} > \mathrm{mean}(T_{3.9\mu m}) + \mathrm{n} \cdot \mathrm{std}(T_{3.9\mu m}) \quad (2)$$

where, $T_{3.9\ \mu m}$ is the 3.9 μm brightness temperature and MaxVar($T_{3.9\mu m}$) and std($T_{3.9\mu m}$) are the maximum variation and the standard deviation, respectively, of the 3.9 μm brightness temperature computed in the 'nonvolcanic' portion of the image. The parameter n controls how much the MIR temperature of the pixel deviates from the mean value: the higher the n, the more sensitive the algorithm. We usually set n to 2. Following these procedures, all of the computations are based on dynamic thresholds that reduce the number of false alarms due to atmospheric conditions. This HOTSAT hotspot detection algorithm has proven to be more reliable than the classical fixed threshold algorithm, as it also detected thermal anomalies at the end of May and in the first days of June, when the activity was lower (see Figure 3).

2.2 Radiative power estimation

The next step for this HOTSAT volcano monitoring system is the derivation of the radiative power at all of the 'hot' pixels. To avoid problems concerning the well-known dual-band dual/three component technique (i.e. to assume the pixel characterized by two or three thermal components, to find a feasible solution for the nonlinear system, etc.), the MIR radiance technique was applied to volcanic eruptions to estimate the radiant flux from satellite data [Wooster et al. 2003]. This is based on an approximation of Plank's Law as a power law. For each hotspot pixel, the radiative power from all of the hot thermal components can be calculated by combining the Stefan-Boltzmann law and Plank's Law approximation, obtaining:

$$Q_{\mathrm{MIR}} = \frac{A_{\mathrm{sampl}}\,\varepsilon\sigma}{\alpha\varepsilon_{\mathrm{MIR}}} \mathrm{L}_{\mathrm{MIR},h} \quad (3)$$

where, Q_{MIR} is the radiative power (W), A_{sampl} is the ground sampling area (m^2), ε is the emissivity, which is a composite value that depends on the mixing ratio of the molten lava and crust, σ is the Stefan-Boltzmann constant ($5.67 \cdot 10^{-8}$ J s^{-1} m^{-2} K^{-4}),

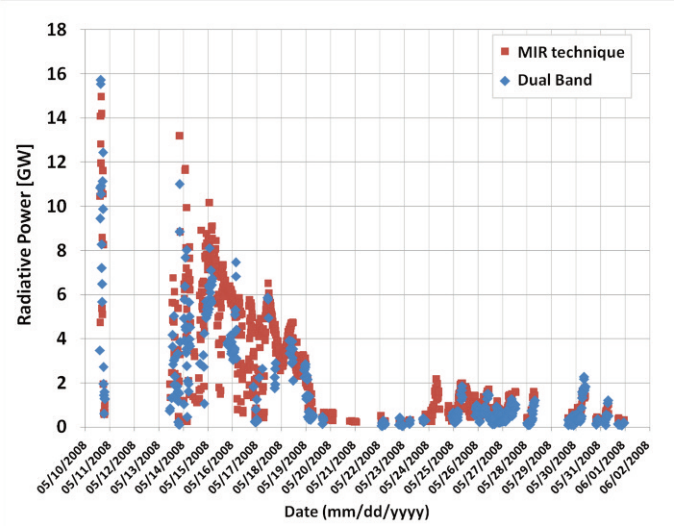

Figure 4. Radiative power computed by the MIR radiance technique (red) and by the dual-band three-component technique (blue) for the SEVIRI data during May, 2008.

$L_{MIR,h}$ and ε_{MIR} are the hot pixel spectral radiance and surface spectral emissivity in the appropriate MIR spectral band, respectively, and the constant a (W m^{-4} sr^{-1} μm^{-1} K^{-4}) is determined from the empirical best-fit relationships.

From Equation (3), the radiant flux is proportional to the calibrated radiance that is associated to the hot part of the pixel, computed as the difference between the observed hotspot pixel radiance in the MIR (3.9 μm) channel and the background radiance that would have been observed at the same location in the absence of thermal anomalies.

To determine the validity of the MIR radiance approach for volcanic eruptions, we compared it to the dual-band technique. Figure 4 shows in the same plot the radiative power computed by the MIR radiance approach (red symbols) and that obtained by the dual-band technique (blue symbols) for the SEVIRI data during May 2008. These computations were made on the same sample of hot pixels without using any default solution for their saturation. Indeed, the nonlinear system of two equations and two unknowns that arises from the dual-band technique was solved as an optimization problem. The results clearly show the good agreement between the two techniques, even if a solution for the nonlinear system is not always found for the dual-band method. This could lead to a loss of information. As the MIR radiance method is a proportionality to the MIR radiance associated to the hot part of the pixel, it does not suffer from this problem, and it is computationally more efficient.

3. Case study: 2008-2009 Etna eruption

The latest effusive eruption on the NE flank of Mount Etna started on May 13, 2008, and ended on July 6, 2009, and this provided an excellent opportunity to determine the performance of HOTSAT in the monitoring of an ongoing eruption. The eruption was preceded by a lava fountain on May 10 from the SEC, and was initiated on May 13 with a system of eruptive fissures that propagated SE from the summit craters towards the western wall of the Valle del Bove. Lava fountains erupted from a N140°E fissure the extended between 3,050 and 2,950 m asl. In two hours, the eruptive fissure propagated downslope and southeastwards, curving N120°E, and reached its minimum altitude of 2,620 m asl [Bonaccorso et al. 2011]. Meanwhile, strombolian activity was displaced from the upper segment of the fissure to its lowest portion. Here, a lava flow erupted at high flow rates from two main vents, and it rapidly expanded into the barren Valle del Bove, where it reached about 6 km in length and the lowest altitude of 1,300 m asl in 24 hours. The most distant lava fronts stagnated about 3 km from the nearest village, Milo.

Volcanic thermal anomalies were observed almost continuously over the same Mount Etna flank in agreement with the occurrence of the lava effusion. We detected the beginning of the lava fountain with SEVIRI-HOTSAT on May 10 at 13:57 GMT, with an initial radiant flux of 4.73 GW. No hotspots were detected with HOTSAT on MODIS, as the two scenes were acquired the same day at 12:40 GMT (Aqua), before the beginning of the lava fountain, and at 20:25 GMT (Terra) after its end. Instead analysis of the SEVIRI data revealed thermal anomalies until 18:57 GMT, which reached a maximum value of about 15 GW at 14:57 GMT (Figure 5). Moreover, at 17:27 GMT, we measured a sharp decrease in the radiative power, which dropped by about 6 GW in 15 min.

In any case, the high sensitivity of the MODIS sensor was significant since it detected the beginning of the eruption on May 13 at 9:50 GMT, when two hot pixels were located that corresponded to the eruptive fissures, almost one hour before SEVIRI. Indeed, the first thermal anomaly by SEVIRI-HOTSAT, due to the eruption was detected on May 13 at 10:27 GMT. This is because the ground-projected area of the SEVIRI instant field of view is more than one

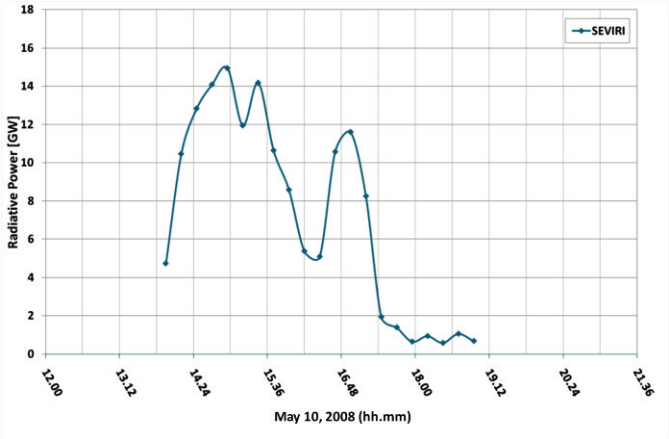

Figure 5. Radiative power computed for the SEVIRI data during the lava fountain that occurred on May 10, 2008.

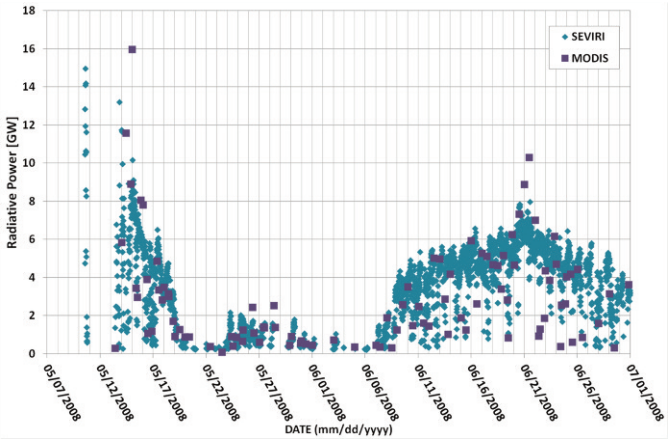

Figure 6. Radiative power computed for the SEVIRI (green) and MODIS (violet) data during May and June, 2008.

order of magnitude greater than that of MODIS, and thus it cannot distinguish such small thermal anomalies as those that are detectable by MODIS [Roberts et al. 2005]. Radiative transfer modeling suggests that SEVIRI should be able to detect and characterize volcanic events where the radiative power ranges from 100 MW to 1,000 MW per pixel, which implies that for the typical range of volcanic eruption temperatures (800-1,000 K), the minimum area detectable should be about 100 m^2 [Roberts et al. 2005].

The largest instantaneous radiant flux of the eruption was about 16 GW, which was observed with MODIS-HOTSAT on May 15, at 00:15 GMT. A comprehensive evaluation of the consistency of the radiant flux measurements carried out on SEVIRI with HOTSAT is shown in Figure 6, with respect to the nearest MODIS scene, during May and June, 2008. It is worth noting how the two time series agree well in confirming the robustness of the HOTSAT system and showing how the synergetic use of MODIS and SEVIRI allows a more precise and almost continuous monitoring of the volcano.

A further advantage of the multiplatform approach is related to sensor saturation problems. The saturation level for the SEVIRI MIR channel is ~335 K, and this necessarily led to errors of underestimation over the most intense phases of the eruptive activity. On the other hand, as MODIS has a much higher saturation temperature (~500 K, band 21), it seldom if ever suffers from the such errors.

By using the consistent radiant flux obtained from HOTSAT on both MODIS and SEVIRI images, it is possible to obtain a chronology of the eruption (that distinguishes different phases) (Figure 6). There was a significant increase in the number of hotspots detected on the morning of May 13, with an evident increase also in their relative intensity. This was recognized in concordance with the opening of the new eruptive fissure on the NE side of the SEC. Ground observations identified the anomaly as due to the lava from the activity that started almost at the same time as the image acquisition [Branca and Andronico 2008].

The strongest phase was revealed by the set of images acquired by both MODIS and SEVIRI up to May 16, with an increase in the thermal anomaly that was centered in the same area of Valle del Bove; this reached the maximum value on May 15 (Figure 6). From May 16, there was a decline in the radiative power that was confirmed by a new change in the structure of the thermal anomaly, with the eastern portion of the anomaly becoming narrower and less intense. This reduction in the radiant flux, and thus in the effusion rates, continuing until June 8, and maintained an average daily value of about 1-2 GW. This was also consistent with field observations of the period [Miraglia 2008]. Finally, an increase in the value of the radiant flux was recorded from June 8 to June 30, which reached a maximum between June 20 and June 21. This behavior might have been due to an increase in the Strombolian activity that was registered during this period.

4. Conclusions

We have presented here HOTSAT, a new automatic system that was specifically developed to elaborate volcanic thermal anomalies. The aim of the system is to integrate real-time satellite observations coming from sensors with different features, in terms of spatial, temporal and spectral resolution. Our thermal system was designed to process satellite data acquired by the MODIS and SEVIRI sensors to detect volcano hotspots and to estimate the associated radiative power. We introduced a new algorithm that is based on a contextual approach, and a variable threshold for the thermal monitoring of volcanoes. Moreover, we computed the radiative power associated to each hot pixel through the MIR radiance technique that was introduced by Wooster et al. [2003] for forest fires.

The ultimate goal of this study is to provide an instrument that can automatically monitor the thermal state of active volcanoes with a refreshing time of 15 min. The preliminary results for the Mount Etna 2008 eruption provide us with strong encouragement to improve this instrument. Indeed, due to the SEVIRI data, it was possible to observe short dynamic activities, such as a paroxysm that preceded the eruption, while with the MODIS images, it was possible to also detect low intensity thermal anomalies.

Moreover, HOTSAT can capture the different phases of the eruptive activity, thereby enabling a detailed chronology of the lava flow emplacement. The good agreement between the radiative power computed from the SEVIRI and MODIS images confirms the reliability of this methodology, as well as the potential of the whole integrated processing chain as an effective tool for real-time monitoring and assessment of volcanic hazard.

Additional products should be available in the near future. The modular architecture ensures straightforward integration for our own algorithms and of those from third parties, as new modules need only to be registered within the control unit module.

Acknowledgements. We are grateful to EUMETSAT for the SEVIRI data and to NASA for the MODIS data. We thank Matthew Blackett and Sergio Pugnaghi for their constructive and helpful comments that greatly improved the manuscript. This study was performed with financial support from the V3-LAVA project (INGV-DPC 2007-2009 contract).

References

Branca, S. and D. Andronico (2008). Eruzione Etna 13 maggio 2008, Aggiornamento attività eruttiva ore 19, Prot. int. n° UFVG2008/044.

Bonaccorso, A., A. Bonforte, S. Calvari, C. Del Negro, G. Di Grazia, G. Ganci, M. Neri, A. Vicari and E. Boschi

(2011). The initial phases of the 2008-2009 Mt. Etna eruption: a multi-disciplinary approach for hazard assessment, J. Geophys. Res., 116, B03203, 19 pp.; doi: 10.1029/2010JB007906

Flynn, L.P., P.J. Mouginis-Mark and K.A. Horton (1994). Distribution of thermal areas on an active lava flow field: Landsat observations of Kilauea, Hawaii, July 1991, B. Volcanol., 56, 284-296.

Francis, P.W. and R. McAllister (1986). Volcanology from space; using Landsat thematic mapper data in the central Andes, EOS, Trans. Am. Geophys. Union., 67, 170-171.

Francis, P.W. and D.A. Rothery (1987). Using the Landsat thematic mapper to detect and monitor active volcanoes: an example from Lascar volcano, northern Chile, Geology, 15, 614-617.

Francis, P.W. and D.A. Rothery (2000). Remote sensing of active volcanoes, Annu. Rev. Earth Planet. Sci., 28, 81-106.

Freeborn, P.H., M.J. Wooster, G. Roberts, B.D. Malamud and W. Xu, (2009). Development of a virtual active fire product for Africa through a synthesis of geostationary and polar orbiting satellite data, Remote Sens. Environ., 113, 1700-1711.

Harris, A., R.A. Vaughan and D.A. Rothery (1995). Volcano detection and monitoring using AVHRR data: the Krafla eruption, 1984. Int. J. Remote Sens., 16, 1001-1020.

Harris, A.J.L. and D. S. Stevenson (1997). Thermal observations of degassing open conduits and fumaroles at Stromboli and Vulcano using remotely sensed data, J. Volcanol. Geoth. Res., 76, 175-198.

Harris, A., S. Blake, D. Rothery and N. Stevens (1997). A chronology of the 1991 to 1993 Mount Etna eruption using advanced very high resolution radiometer data: implications for real-time thermal volcano monitoring, J. Geophys. Res., 102, 7985-8003.

Harris, A.J.L., L.P. Flynn, L. Keszthelyi, P.J. Mouginis-Mark, S.K. Rowland and J.A. Resing (1998). Calculation of lava effusion rates from Landsat TM data, B. Volcanol., 60, 52-71.

Harris, A.J.L., L.P. Flynn, D.A. Rothery, C. Oppenheimer and S.B. Sherman (1999). Mass flux measurements at active lava lakes: implications for magma recycling. J. Geophys. Res. 104, 7117-7136.

Harris, A.J.L., J.B. Murray, S.E. Aries, M.A. Davies, L.P. Flynn, M.J. Wooster, R. Wright and D.A. Rothery (2000). Effusion rate trends at Etna and Krafla and their implications for eruptive mechanisms, J. Volcanol. Geoth. Res., 102, 237-270.

Harris, A., J. Dehn and S. Calvari (2007). Lava effusion rate definition and measurement: a review, B. Volcanol.; doi: 10.1007/s00445-007-0120-y.

Hérault, A., A. Vicari, A. Ciraudo and C. Del Negro (2009). Forecasting lava flow hazards during the 2006 Etna eruption: Using the MAGFLOW cellular automata model, Comput. Geosci.-UK, 35 (5), 1050-1060; doi: 10.1016/j.cageo.2007.10.008.

Higgins, J. and A.J.L Harris (1997). VAST: a program to locate and analyze volcanic thermal anomalies automatically from remotely sensed data, Comput. Geosci-UK, 23 (6), 627-645.

Hirn, B., C. Di Bartola and F. Ferrucci (2005). Automated, multi-payload, high-resolution temperature-mapping and instant lava-effusion-rate determination at erupting volcanoes, 2005 IEEE International Geoscience & Remote Sensing Symposium (Seoul, Korea, July 25-29).

Hirn, B., C. Di Bartola, G. Laneve, E. Cadau and F. Ferrucci (2008). SEVIRI onboard Meteosat Second Generation, and the quantitative monitoring of effusive volcanoes in Europe and Africa, 2008 IEEE International Geoscience & Remote Sensing Symposium (Boston, Massachusetts, U.S.A, July 6-11).

Kaneko, T., M.J. Wooster and S. Nakada (2002). Exogenous and endogenous growth of the Unzen lava dome examined by satellite infrared image analysis, J. Volcanol. Geoth. Res. 116, 151-160.

Kaufman, Y.J. , C.O. Justice, L.P. Flynn, J.D. Kendall, E.M. Prins, L. Giglio, D.E.Ward, W.P.Menzel and A.W. Setzer (1998). Potential global fire monitoring from EOS-MODIS, J. Geophys. Res., 103, 32215-32238.

Laneve, G. and E.G. Cadau (2009). Quality assessment of the fire-hazard forecast based on a fire potential index for the Mediterranean area by using a MSG/SEVIRI based fire detection system, In: Geoscience and Remote Sensing Symposium, 2007. IGARSS 2007. IEEE International (23-28 July 2007), 2447-2450; doi: 10.1109/IGARSS.2007.4423337.

Miraglia, L. (2008). Rapporto settimanale sull'attività eruttiva dell'Etna (2-8 giugno, 2008), Prot. Int. n° UFVG2008/057.

Oppenheimer, C. (1991). Lava flow cooling estimated from Landsat thematic mapper infrared data: the Lonquimay eruption (Chile, 1989), J. Geophys. Res., 96, 21865-21878.

Roberts, G., M.J. Wooster, G.L.W. Perry, N. Drake, L.-M. Rebelo and F. Dipotso (2005). Retrieval of biomass combustion rates and totals from fire radiative power observations: application to southern Africa using geostationary SEVIRI imagery, J. Geophys. Res., 110, D21111; doi: 10.1029/2005JD006018.

Vicari, A., A. Ciraudo, C. Del Negro, A. Hérault and L. Fortuna (2009). Lava flow simulations using discharge rates from thermal infrared satellite imagery during the 2006 Etna eruption, Nat. Hazards, 50, 539-550; doi: 10.1007/s11069-008-9306-7.

Wooster, M.J., B. Zhukov and D. Oertel (2003). Fire radiative energy for quantitative study of biomass burning:

derivation from the BIRD experimental satellite and comparison to MODIS fire products, Remote Sens. Environ., 86, 83-107.

Wright, R., S. Blake, A. Harris and D. Rothery (2001). A simple explanation for the space-based calculation of lava eruption rates, Earth Planet Sci. Lett. 192, 223-233.

Wright, R., L. Flynn, H. Garbeil, A. Harris and E. Pilger (2002). Automated volcanic eruption detection using MODIS, Remote Sens. Environ. 82, 135-155.

Wright, R., L.P. Flynn, H. Garbeil, A.J.L. Harris and E. Pilger (2004). MODVOLC: near-real-time thermal monitoring of global volcanism, J. Volcanol. Geoth. Res. 135, 29-49.

*Corresponding author: Gaetana Ganci,
Istituto Nazionale di Geofisica e Vulcanologia, Sezione di Catania,
Osservatorio Etneo, Catania, Italy; email: gaetana.ganci@ct.ingv.it.